coatings

MDPI

Article

The Mechanism of the Interaction Between Dodecylbenzene Sulfonate and TiO_2 Surfaces—DFT Study

Yujie Song [1], Lei Xia [1,*], Xueting Zhang [1], Yan Li [2], Fulin Wang [1] and Xue Li [1]

[1] School of Material and Metallurgy, University of Science and Technology Liaoning, Anshan 114051, China
[2] Delin Land Port Supply Chain Services Co., Ltd., Ansteel Group Corporation, Anshan 114009, China
* Correspondence: xialei0627@163.com

Highlights

What are the main findings?

- DBS^- prefers to adopt a configuration in which it is lying (−210.29 kJ/mol) on a TiO_2 surface via synergistic sulfonate coordination, benzene π-interaction, and alkyl van der Waals forces.
- Sulfonate acts as the key active site, forming Ti-O bonds powered by negative electrostatic potential and high Fukui values.
- The benzene ring serves as an electron acceptor, providing auxiliary stability through weak π-d coupling with surface Ti atoms.

What is the implication of the main findings?

- Adsorption induces 0.7 e electron transfer from DBS^- to TiO_2, as confirmed by O 2p and Ti 3d orbital overlap.

Abstract

To elucidate the microscopic adsorption mechanism of dodecylbenzenesulfonate (DBS^-) on the surface of anatase TiO_2, this study was conducted based on density functional theory, using the $DMol^3$ module for calculations. Four representative initial configurations including orientation differences in sulfonate, the benzene ring, and the alkyl chain were constructed. The contribution of each functional fragment to adsorption stability and interfacial electron transfer behavior were investigated through geometric optimization, energy calculation, Mulliken population, molecular electrostatic potential analysis, Fukui function, and density-of-states analysis. The results showed that configuration a-101 exhibited a lying orientation and multi-stage synergetic adsorption, with the largest adsorption energy (−210.29 kJ/mol), and it was the most stable configuration. The sulfonate group had the most negative electrostatic potential, and the highest occupied orbital was mainly located on its oxygen atom (O). Additionally, the f^- value of the Fukui function of O was the highest, serving as the key electrophilic reaction active site, and formed a Ti-O coordination bond with surface Ti^{4+}. The benzene ring acted as an electron acceptor and participated in adsorption through π-d weak coupling. Adsorption induced the transfer of an about 0.7 e charge from DBS^- to TiO_2. The 2p orbitals of O and the 3d orbitals of Ti overlapped in the range of −5.0~0.45 eV, forming a coordination bond.

Keywords: dodecyl benzene sulfonate; titanium dioxide; adsorption mechanism; electron transfer; interfacial interaction

Check for updates

Academic Editor: Andrey V. Osipov

Received: 24 December 2025
Revised: 22 January 2026
Accepted: 25 January 2026
Published: 30 January 2026

Copyright: © 2026 by the authors. Licensee MDPI, Basel, Switzerland. This article is an open access article distributed under the terms and conditions of the Creative Commons Attribution (CC BY) license.

1. Introduction

With the development of nanotechnology, titanium dioxide (TiO_2) has become an important functional material due to its excellent photocatalytic properties, ultraviolet-shielding properties, and high chemical stability, and it is widely used in cosmetics, coatings, environmental purification, new energy, metal processing and lubrication, and other fields [1–3]. In particular, in the field of coatings, TiO_2 is widely employed in high-performance protective coatings, decorative coatings, and photocatalytic self-cleaning coatings owing to its high refractive index, photoaging resistance, and anti-corrosion characteristics. It can not only enhance the mechanical strength and durability of coatings but also endow coatings with UV resistance, anti-pollution, and environmental purification functions [4,5].

However, in practical applications, nano TiO_2 exhibits a strong tendency to agglomerate due to its high surface energy [6]. The agglomerates result in a loss of the nano-effect, leading to a dramatic decrease in performance. In order to improve this situation, researchers have tried to introduce various surfactants to modify the surface properties of TiO_2. Sodium dodecyl benzene sulfonate (SDBS), a widely used anionic surfactant, demonstrates considerable potential in modifying TiO_2 due to its excellent dispersion stability and interfacial activity [7,8]. SDBS molecules can be dissociated into dodecylbenzene sulfonate (DBS^-) and Na^+ in an aqueous solution, wherein DBS^- possesses a polar head group of sulfonate, a π-conjugated unit of a benzene ring, and a hydrophobic long-chain structure, enabling it to interact with nanoparticles in multiple ways to increase the net surface charge, thereby regulating the surface wettability of TiO_2 and inhibiting particle agglomeration [9].

Du and Guo discussed the influence of SDBS on the aggregation behavior of TiO_2 nanoparticles and found that SDBS could reduce the interfacial tension between TiO_2 particles and the surrounding medium, thereby significantly enhancing the dispersibility and stability of TiO_2 nanoparticles and reducing agglomeration by enhancing electrostatic and spatial repulsion. Utilizing dynamic light scattering and Zeta potential measurement, the mechanism of action of SDBS concentration with respect to the dispersion stability of TiO_2 was analyzed. It was found that the mass ratio of SDBS to TiO_2 was in the optimal range, and an excessive mass ratio might lead to re-agglomeration [10,11]. Sun et al. [12] found that with an increase in SDBS concentration, the absolute value of Zeta potential increased, the average particle size decreased, and agglomeration decreased. An increase in SDBS concentration (0–30 mg/L) significantly enhanced the migration performance of TiO_2. The adsorption capacity of SDBS on TiO_2 surface was significantly affected by pH. The surface was positively charged and the adsorption capacity increased with a decrease in pH when the pH was lower than the isoelectric point. Conversely, when the pH exceeded the isoelectric point, the surface became negatively charged, resulting in a sharp decline in adsorption capacity [13].

Although the application of DBS^- in dispersing TiO_2 has been extensively validated through experiments, at present, the domestic and international research has mainly focused on the dispersal effects of nano-TiO_2 and its influence on the migration ability, corrosion behavior, photochemical activity, thermal conductivity, and tribological performance of nanoparticles [14–17]. The adsorption behavior of DBS^- on the surface of TiO_2 can be indirectly inferred through the measurement of macroscopic kinetic parameters, such as adsorption isotherms and Zeta potential. However, a systematic understanding of the micro-adsorption mechanism and structure–activity relationship of DBS^- on the surface of TiO_2 is lacking, making it difficult to analyze each functional fragment of DBS^- (sulfonate, the benzene ring, and the alkyl chain) at the atomic level. Furthermore, the mechanism of electron transfer between DBS^- and TiO_2 has not been addressed. First-principles analysis can start from the fundamental level, such as the electrical structure, to

elucidate the nature of the interaction between the two, accurately calculate adsorption energy and other key parameters, and thoroughly explore the microscopic interactions between the dispersant and nanoparticle surface, thereby providing a reliable theoretical foundation for optimizing the dispersion system [18–20]. Therefore, a first-principles method based on density functional theory (DFT) was adopted to systematically construct four representative initial adsorption configurations of DBS^- on the anatase TiO_2 (101) surface, which correspond to four possible modes: multi-segment synergy, segment contact, head group anchoring, and benzene ring parallelism. The stability differences of different configurations, the distribution of active sites of DBS^-, and electron transfer between the DBS^- and TiO_2 interface were revealed by means of multi-scale calculations, such as geometric optimization, energy calculation, charge population, density of states (DOS), and partial wave density of states (PDOS) analysis to elucidate the nature of the interaction between DBS^- and the surface of TiO_2 at the atomic/electronic level.

2. Materials and Methods

This research was primarily conducted using the $Dmol^3$ module within the Materials Studio 8.0 platform. DBS^- was constructed, and its structure is shown in Figure 1. The most stable and most frequently exposed crystal plane in anatase TiO_2 (101) [21,22] was selected as the representative research object, and a periodic supercell structure with dimensions of 2.178 nm × 3.020 nm × 2.640 nm was created, which contained three layers of atoms. To maintain lattice stability, the bottom two layers of atoms were fixed, while the coordinates of the upper atoms were fully relaxed during structural optimization. In order to prevent mutual interference between adjacent crystal planes in the periodic structure, a 1.5 nm vacuum layer was introduced in the vertical direction, ensuring the structural independence and calculation accuracy of the system.

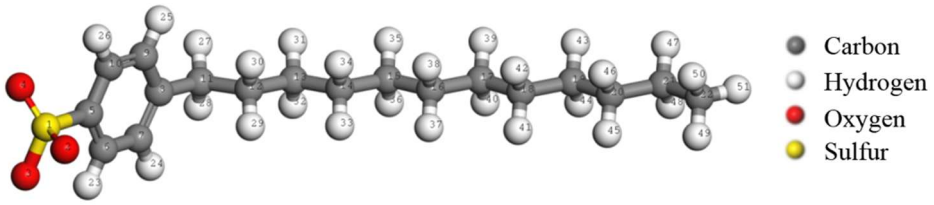


Figure 1. Structure and atomic numbering of DBS^-.

To investigate the adsorption characteristics of DBS^- on the TiO_2 (101) crystal surface, four representative initial adsorption configurations were systematically constructed; this was followed by structure optimization and energy calculations. As illustrated in Figure 2, the differences in these four configurations (a-101, b-101, c-101, and d-101) were mainly reflected in the different initial orientations of the functional fragments of DBS^- (sulfonate head group, benzene ring, and alkyl chain) relative to the crystal plane. This approach was intended to allow us to comprehensively evaluate the synergistic or independent contributions of each fragment to the adsorption process. Through geometric optimization, the most stable adsorption conformations of the four configurations were obtained, and the adsorption energy was calculated using the following formula [23,24] to evaluate the most stable adsorption state.

$$E_{ads} = E_{total} - E_{slab} - E_{adsorben} \quad (1)$$

where E_{total}, E_{slab}, and $E_{adsorben}$ are the total energy of the adsorption system, the energy of the TiO_2 (101) crystal plane, and the energy of DBS^-.

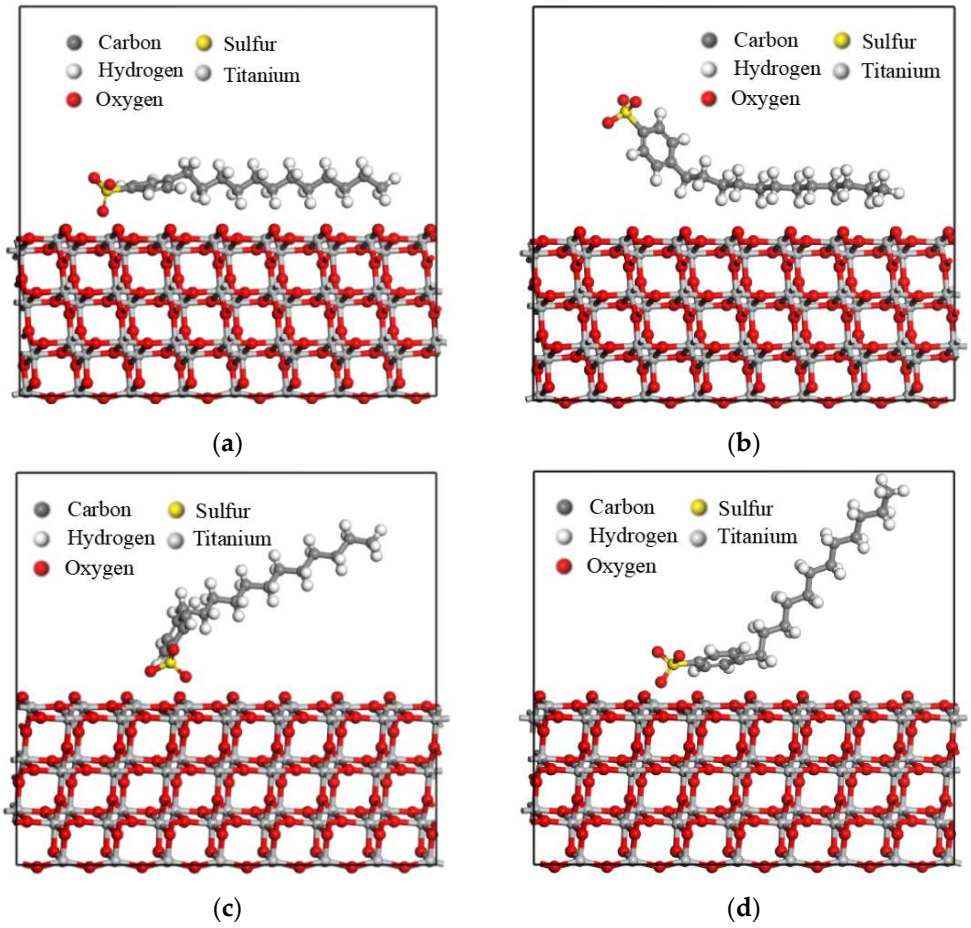


Figure 2. DBS^- adsorbed configurations on TiO_2 (101) crystal plane: (**a**) a-101, (**b**) b-101, (**c**) c-101, and (**d**) d-101.

To elucidate the mechanism through which DBS^- adopts the most stable adsorption configuration on the surface of TiO_2, identify its active sites, and reveal the electronic-structure-based origin of its specific adsorption configuration stability, the nature of the interaction between DBS^- and the surface of TiO_2 was systematically studied by using the DFT calculation method. Potential nucleophilic/electrophilic active sites in DBS^- were accurately determined via calculation using the Fukui function and frontier orbitals and molecular electrostatic potential analysis [25,26]. Furthermore, charge transfer behavior during the adsorption process was quantitatively analyzed by comparing the changes in the Mulliken charge populations of key atoms in the model before and after adsorption. The density of states (DOS) of the surface model before and after adsorption was calculated to investigate the impact of DBS^- adsorption on the surface electronic structure of TiO_2 and elucidate the mechanism of electron transfer at the interface.

The relevant calculations are based on the Perdew–Burke–Ernzerhof (PBE) functional under the generalized gradient approximation (GGA), and the all-electron processing method was adopted to accurately describe the electron distribution and local electron response characteristics [27,28]. The basis cutoff radius was set at 4.4 Å, and Grimme DFT-D dispersion correction was introduced to fully consider potential weak van der Waals interactions between molecules and between molecules and surfaces. The convergence conditions were energy variation less than 1×10^{-6} Ha, maximum force less than 2×10^{-3} Ha/Å, and maximum displacement less than 5×10^{-3} Å. In this iterative process, we used the Broyden–Fletcher–Goldfarb–Shanno algorithm to achieve energy minimization. For potential unpaired electrons or spin effects, spin-unconstrained calculations were used

to accurately describe the electron distribution and active site characteristics. The electron integration accuracy and self-consistent field SCF convergence conditions were set to the convergence threshold of 1×10^{-6} Ha. DIIS and preprocessors were enabled to accelerate convergence, while thermal broadening was enabled to assist convergence to ensure the stability of geometric optimization and the reliability of the calculation results.

3. Results and Discussion

3.1. Adsorption of DBS^- on the Surface of TiO_2

The adsorption energies of four representative DBS^- configurations on the TiO_2 crystal surface were calculated to study the stable adsorption states of DBS^- on the surface of TiO_2 and the contributions of various functional fragments, and the results are shown in Table 1.

Table 1. Adsorption energies of different adsorption configurations.

	E_{ads} (kJ/mol)	E_{total} (kJ/mol)	E_{slab} (kJ/mol)	$E_{adsorben}$ (kJ/mol)
a-101	−210.29	−1,347,941.58	−69.54	−1,347,833.26
b-101	−35.77	−1,347,879.24	−60.17	−1,347,783.30
c-101	−163.76	−1,347,995.89	−66.53	−1,347,765.64
d-101	−177.15	−1,347,944.51	−71.63	−1,347,695.73

It can be seen from Table 1 that the adsorption energy for configuration b-101 is the lowest, measuring only −35.77 kJ/mol. This outcome is due to a single adsorption-driving force: the non-polar interaction between the hydrophobic dodecyl chain and the TiO_2 surface. This configuration simulates the potential orientation of the hydrophobic tail toward the surface during surfactant self-assembly, which is less thermodynamically stable. In contrast, the adsorption energy for configuration c-101 is −163.76 kJ/mol, reflecting the specific interaction between the sulfonate head group and the TiO_2 surface. In this arrangement, the oxygen atom of the sulfonate establishes a stable coordination bond with the Ti atom on the surface. This coordination pattern is typical of chemisorption, driven by strong electrostatic attraction and orbital hybridization between the negative charge of the sulfonate and the vacant d orbitals of the surface Ti atoms. This configuration reveals the microscopic mechanism by which DBS^- anchors to the oxide surface via its polar head group. The adsorption energy for configuration d-101 is −177.15 kJ/mol. In addition to the coordination between the sulfonate head group and the TiO_2 surface, the benzene ring is adsorbed parallel to the TiO_2 surface. Compared to configuration c-101, the adsorption strength is slightly greater, indicating that while there is some π-interaction between the aromatic ring and the surface, the interaction is significantly weaker than the coordination effect of the head group. The adsorption energy of configuration a-101 reached −210.29 kJ/mol, indicating a strong chemisorption process. In this configuration, DBS^- does not interact with the surface as a singular entity but rather assumes a lying-down posture, facilitating multi-stage synergistic adsorption of the sulfonate, benzene ring, and alkyl chain. This synergistic effect maximizes the contact area between the molecules and the surface, resulting in the formation of the strongest interaction network. The O atom of the sulfonate establishes a stable coordination bond with the Ti atom on the surface, while π-interaction occurs between the benzene ring and the surface. Additionally, the long alkyl chain extends across the surface through Van der Waals forces. This mode of multi-point anchoring significantly enhances the stability of adsorption.

The adsorption energy for configuration c-101 significantly exceeds that of b-101, suggesting that the coordination bond between the sulfonate head group and the surface Ti atom is the most crucial and stable interaction facilitating adsorption. When multiple

functional fragments (the head group, aromatic ring, and alkyl chain) can simultaneously interact with the surface effectively (as observed in configuration a-101), the adsorption energy is markedly increased, showing an obvious synergistic effect. The adsorption mechanism of DBS^- on the TiO_2 surface can be characterized as head-group-dominant with multi-stage cooperation.

3.2. DBS^- Active Site Analysis

The electrostatic potential, frontier orbitals, and Fukui function of DBS^- were calculated to identify the reactive sites of DBS^- during the adsorption process. The distribution of electrostatic potential serves as a crucial metric for characterizing the charge properties of various regions within the molecule, effectively reflecting the initial tendencies of the interaction of DBS^- with the surface. The electrostatic potential distribution of DBS^- is shown in Figure 3.

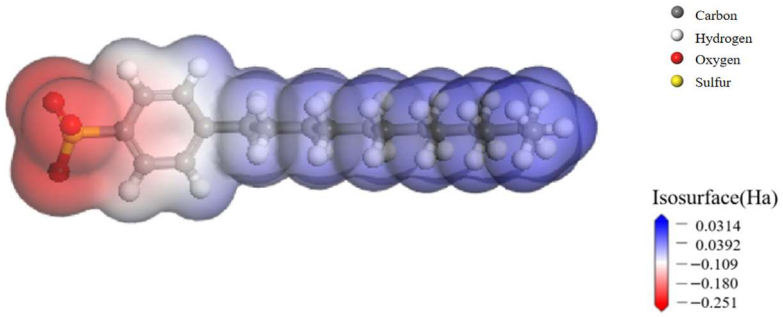
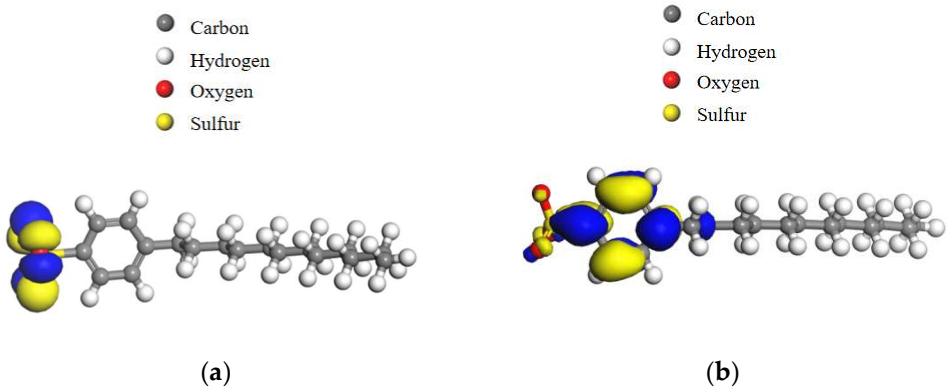


Figure 3. Electrostatic potential distribution of DBS^-.

Figure 3 illustrates that the sulfonate group region exhibits a significant negative potential, creating an outward-expanding equipotential surface. This observation indicates the presence of a highly localized and continuous negative charge region in this area. The strong negative potential region easily adsorbs or coordinates with sites with positive charges on the surfaces of metal oxides (such as Ti atoms). The emergence of this negative potential can mainly be attributed to two factors. First, the electron-induced effect between the S=O and S–O bonds within the sulfonate group leads to the delocalization of electrons around oxygen atoms, thereby establishing a stable electron-rich structure. Second, DBS^- itself functions as a negatively charged ionic group, endowing it with inherent electrostatic adsorption capabilities. In contrast, the benzene ring and the dodecyl segments in DBS^- do not exhibit significant potential polarization characteristics. The weak negative potential observed in the benzene ring region can be attributed to the delocalization of π electrons within the aromatic benzene ring structure, which generates an electron cloud characterized by a uniform spatial distribution but low intensity. Due to its non-polarity and uniform electron distribution, the long-chain alkyl structure does not serve as an electron-rich or an electron-deficient region, resulting in a diminished capacity for electrostatic interaction with the surfaces of metal oxides. Consequently, rather than functioning as electronically active adsorption sites, the role of alkyl chains in the adsorption process is primarily governed by non-polar Van der Waals interactions.

Frontier orbital analysis is an electronic structure research method based on molecular orbital theory. By assessing the spatial distribution of the highest occupied molecular orbital (HOMO) and the lowest unoccupied molecular orbital (LUMO), this method elucidates molecular electronic distribution, trends in electron transfer, and potential mechanisms of interaction with external systems [29–31]. The results of the frontier orbital analysis for DBS^- are shown in Figure 4. As depicted in Figure 4, the HOMO of DBS^- is predominantly localized in the oxygen atom region of the sulfonate group (Figure 4a). This localization is

a product of the contribution of the lone-pair electrons on the oxygen atom, indicating that the region possesses a strong electron donor capacity, which is conducive to electrostatic interactions or coordination adsorption with metal sites on the surfaces of metal oxides. Conversely, the LUMO of DBS^- is primarily concentrated in the benzene ring region, indicating that the benzene ring exhibits electron acceptor characteristics and may engage in π-d interactions with d orbitals of the TiO_2 surface metal. The spatial distribution of HOMO and LUMO provides DBS^- with a regionalization function during the adsorption process. The sulfonate group primarily enhances adsorption stability, whereas the benzene ring region is involved in regulating molecular polarization and interfacing. Furthermore, the long alkyl segment exhibits a negligible frontier orbital distribution and does not participate in the reaction.



(**a**) (**b**)

Figure 4. (**a**) HOMO and (**b**) LUMO distribution of DBS^-.

To further quantify the local reactivity of DBS^-, a Fukui function analysis was conducted, and the results are shown in Table 2. The f^- value mainly reflects the active site of the molecule during electrophilic reactions, while the f^+ value indicates the active site, which is easily attacked by nucleophilic reactions. A larger value corresponds to greater reactivity. As shown in Table 2, the three oxygen atoms in the sulfonate group (O2, O3, and O4) show significantly higher and comparable f^- values (0.242, 0.248, and 0.250, respectively), confirming that this region serves as the key electron donor active site. This finding aligns with its high HOMO contribution. These oxygen atoms are highly sensitive to variations in electron density and exhibit strong and balanced nucleophilic reactivity due to the resonance effect and electron delocalization within the sulfonate group, thereby facilitating the adsorption and coordination of DBS^- on the metal oxide surface. In contrast, the f^+ values at specific carbon atoms of the benzene ring (C5, C8, and C10) show higher values (0.103, 0.115, and 0.101, respectively), significantly higher than the rest of the atoms on the benzene ring, indicating that these sites exhibit relative nucleophilicity. This distribution characteristic is also consistent with the corresponding LUMO contribution rate. C5 (carbon bonded to the sulfonate), C8 (the para-carbon of C5), and C10 (the ortho-carbon of C5) are located in the conjugated electron transport pathway of the benzene ring. The strong electron-withdrawing induction effect of the sulfonate group, in conjunction with the π-conjugation effect of the benzene ring, synergistically enhances the reaction sensitivity of the carbon atoms within an electron-rich environment.

Table 2. Contribution rates of HOMO and LUMO and Fukui function values of atoms in DBS^-.

Atom	HOMO Contribution Rate	LUMO Contribution Rate	f^-	f^+
S1	0.00	0.02	0.104	0.036
O2	0.33	0.03	0.242	0.039

Table 2. *Cont.*

Atom	HOMO Contribution Rate	LUMO Contribution Rate	f^-	f^+
O3	0.32	0.01	0.248	0.042
O4	0.32	0.02	0.250	0.037
C5	0.01	0.29	−0.004	0.103
C6	0.00	0.06	0.014	0.057
C7	0.00	0.09	0.009	0.076
C8	0.00	0.28	0.014	0.115
C9	0.00	0.02	0.010	0.037
C10	0.00	0.14	0.010	0.101
C11	0.00	0.00	−0.003	−0.019
C12	0.00	0.03	−0.003	−0.016
C13	0.00	0.00	−0.001	−0.003

3.3. Electron Transfer Mechanism at Adsorption Interface

The charge transfer in the adsorption process serves as a critical parameter for assessing stability and interaction strength. The Mulliken charge of DBS^- and the density of states (DOS) distribution on the TiO_2 surface both before and after adsorption were analyzed to investigate the mechanism of electron transfer between DBS^- and TiO_2. Previous studies indicate that the active site for electron interaction primarily resides within the sulfonate and benzene ring structures, while the alkyl chain does not participate. To streamline the model and conserve computational resources, this analysis focuses solely on the sulfonate group and the benzene ring. The Mulliken charge of DBS^- before and after adsorption is shown in Figure 5. Initially, the total charge of DBS^- is −1 e before adsorption, reflecting its anionic nature. The total charge changes to approximately −0.3 e after adsorption. This indicates that about 0.7 e electrons are transferred from DBS^- to the TiO_2 surface, indicating notable interfacial electron migration. The local charge distribution in DBS^- also undergoes modification. Prior to adsorption, the sulfur atom in the sulfonate group possesses a charge of +1.626 e, while the charges of the three oxygen atoms are uniformly distributed between −0.812 e and −0.817 e. Following adsorption, the charge of the sulfur atom decreases to +1.533 e (indicating an increase in electron density), whereas the charges of the oxygen atoms shift to a range of −0.674 e to −0.752 e (reflecting a decrease in electron density). This change suggests that the adsorption of DBS^- on the TiO_2 surface induces a rearrangement of intramolecular electrons, with the electrons transferred from DBS^- primarily originating from the oxygen atom in the sulfonate group. Its high electronic activity makes it the main electron donor site. The previous analyses of the HOMO orbit and Fukui function of DBS^- are thus corroborated.

The charges of the carbon and hydrogen atoms in the benzene ring exhibited significant changes before and after adsorption, indicating that the polarization effect in the adsorption process extends beyond the sulfonate region. This effect propagated to the far-end structure of the molecule via the internal conjugated system. In the electron cloud distribution differential charge diagram of the TiO_2 surface and DBS^- interface (Figure 6), it can be seen that obvious electron cloud overlap occurred between the sulfonate oxygen atom and Ti atom on the TiO_2 surface. This localized electron coupling microscopically confirms the transfer of electrons between DBS^- and the TiO_2 surface, which is crucial for the stability of their adsorption. The observed electron transfer reveals the overall electron exchange process between DBS^- and the TiO_2 surface, while the electron cloud overlap substantiates the bonding characteristics of the coordination bond. Both explain the evolution of the electronic structure and the essential reason for stable adsorption in the process of adsorption.

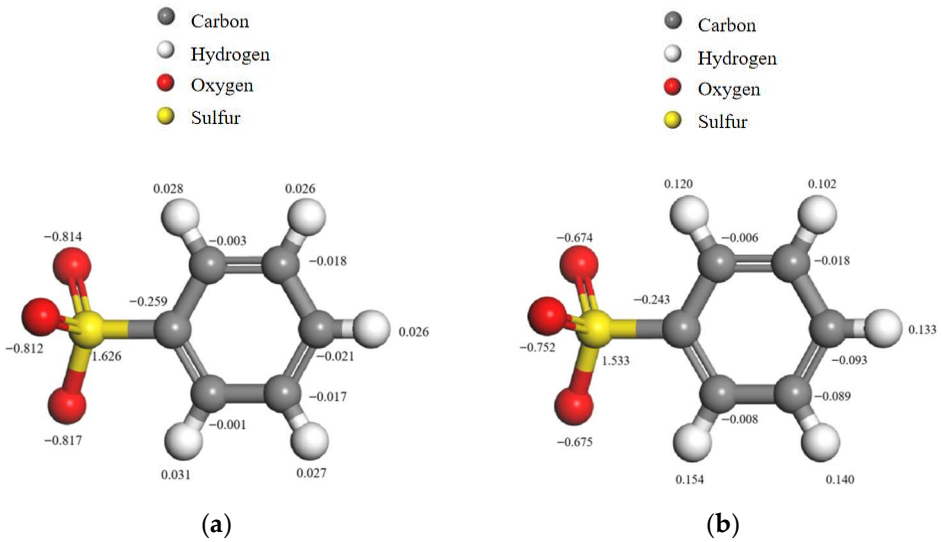


Figure 5. Change in Mulliken charge before and after DBS^- adsorption: (**a**) before adsorption and (**b**) after adsorption.

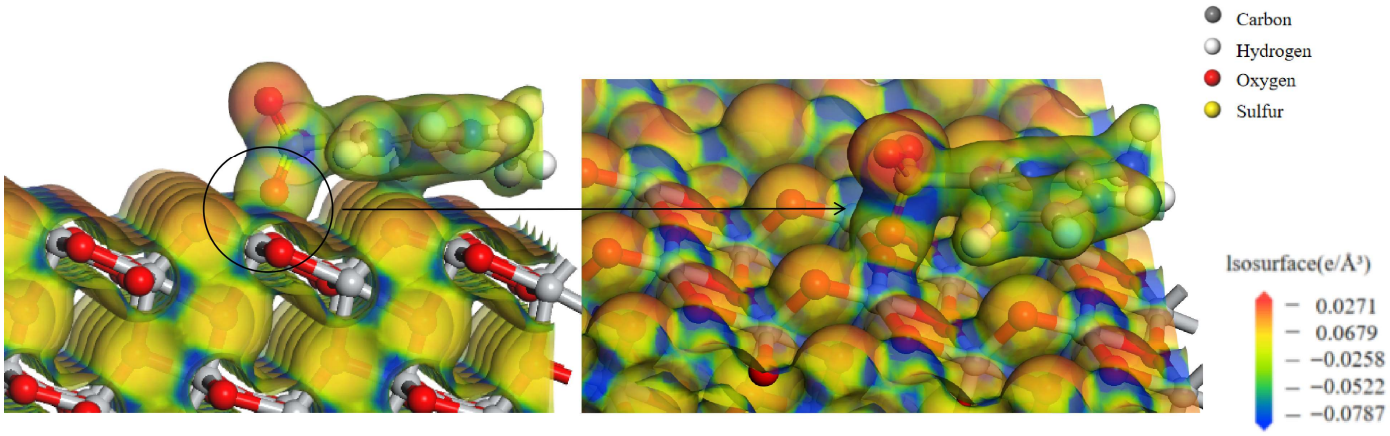


Figure 6. Differential charge diagram of the TiO_2 surface with the DBS^- interface.

To explore the influence of DBS^- adsorption on the electronic structure of the TiO_2 surface, the DOS distribution of the TiO_2 surface before and after adsorption was analyzed, as illustrated in Figure 7. The results show that there is significant energy domain dependence in the three characteristic energy regions. Notably, the DOS spectra at the deep energy levels (−17.50 to −15.00 eV) exhibit minimal changes, indicating that the electrons in the inner layer do not participate in the adsorption process. In the valence band (−5.00~0.95 eV), the decrease near the Fermi level indicates a reduction in available electronic states. At the same time, the peak position of the conduction band has shifted toward lower energy levels, which indicates that the energy level of the conduction band has decreased. The above alterations demonstrate that the adsorption leads to a reduction in electronic energy and available density of states, indicating a tendency toward greater stability in the electronic configuration. This evidence supports the conclusion that DBS^- adsorption exerts a stabilizing effect on the electronic structure of the surface of TiO_2.

To further elucidate the electronic coupling mechanism between DBS^- and the TiO_2 surface, the partial density of states (PDOS) between the key atoms was calculated, as shown in Figure 8. Notably, there is a significant orbital overlap between the 2p orbital of the O atom in DBS^- and the 3d orbital of the surface Ti atom within the energy range of −5.0~0.45 eV. Combining this information with the characteristics of the electron cloud overlap further confirms that the formation of the coordination bond between these atoms

is the primary contributor to adsorption (Figure 8a). Additionally, the C atomic orbitals of the benzene ring in DBS^- also exhibit an overlap with the Ti atoms in this energy range (Figure 8b). Despite the extensive overlapping area in the DOS, there is no coincidence of electron clouds between the orbital spatial distributions (Figure 6). Consequently, no significant bonding effect can be observed. Instead, this interaction manifests as a weak π–d orbital coupling. The 1s orbital of the hydrogen atom and the 2p orbital of the surface oxygen atom exhibit an overlap in orbital density of states within the energy range of −5 to 0 eV (Figure 8c), indicating the presence of weak orbital coupling. This interaction can regulate the interface local electron density distribution and energy level structure, consequently impacting the electron transport process and local charge distribution. This phenomenon primarily accounts for the decrease in electron density of the hydrogen atom on the benzene ring after adsorption. Conversely, the overlap in the DOS between the S atom and the Ti and O atoms appears minimal (Figure 8d), reflecting the limited electron involvement of the S atom. Its primary role lies in aiding stability and electronic regulation rather than engaging in substantial electronic coupling or bonding.

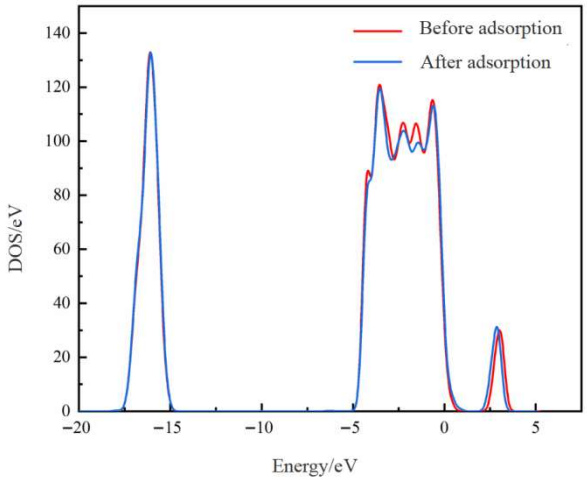
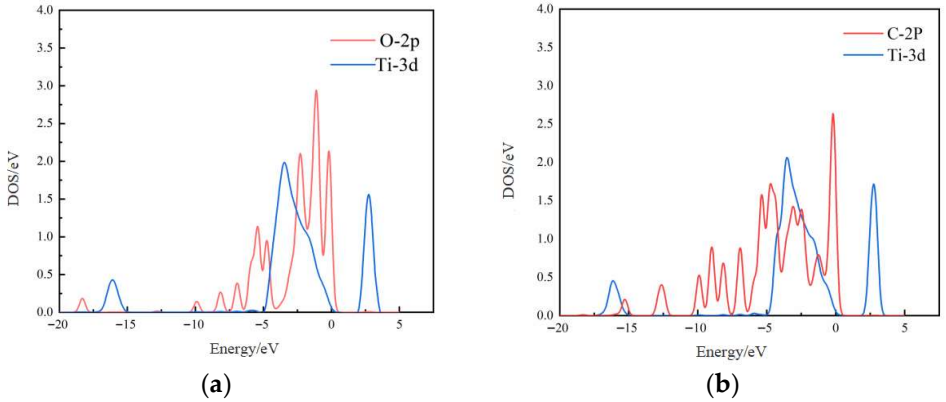
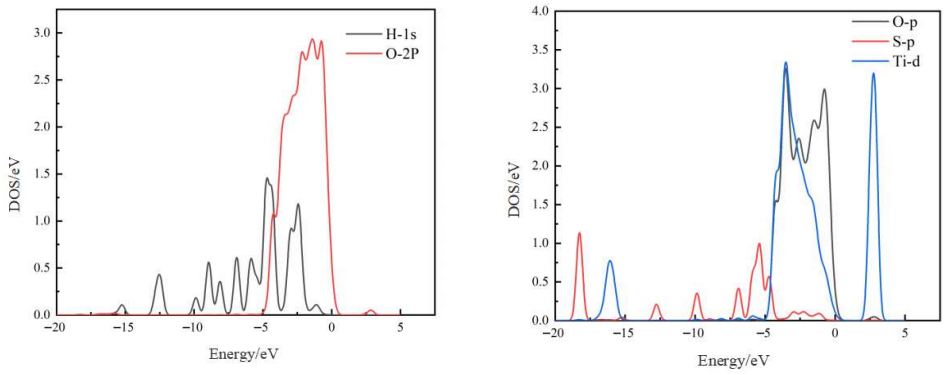


Figure 7. DOS of TiO_2 (101) crystal plane before and after adsorption.



(**a**) (**b**)

Figure 8. *Cont.*



(**c**) (**d**)

Figure 8. PDOS overlap: (**a**) O in DBS^- and Ti in TiO_2, (**b**) C in DBS^- and Ti in TiO_2, (**c**) H in DBS^- and O in TiO_2, and (**d**) S in DBS^- and O and Ti in TiO_2.

4. Conclusions

(1) The most stable configuration of DBS^- on the surface of TiO_2 is one where DBS^- is lying on the TiO_2 surface. This configuration realizes strong multi-site adsorption through sulfonate-Ti coordination, benzene ring–surface π interaction, and non-polar Van der Waals interactions between the alkyl chain and the surface. The adsorption energy is −210.29 kJ/mol, which is consistent with chemisorption characteristics.

(2) The electrostatic potential of the sulfonate group on DBS^- is negative, the HOMO is primarily localized on the oxygen atom of the sulfonate group, and the Fukui function f^- value of the oxygen atom is high, indicating that it serves as the principal site for nucleophilic reactions and governs the electron donor behavior. In contrast, the benzene ring acts as an electron acceptor, which regulates interfacial matching through π-d weak coupling, while the alkyl chain exhibits minimal electronic activity.

(3) Adsorption induces the transfer of 0.7 e electrons from DBS^- to the TiO_2 surface. This electron transfer primarily originates from the oxygen atom in the sulfonate group. PDOS analysis showed that O in DBS^- and Ti on the TiO_2 surface produce a strong overlap of orbitals and an electron cloud, forming a coordination bond. Although the overlap area in DOS between C on the benzene ring of DBS^- and Ti is substantial, there is no corresponding electron cloud overlap, leading to only weak π-d coupling.

Author Contributions: Conceptualization, L.X., Y.L., and X.L.; methodology, L.X., Y.L., and X.L.; formal analysis, Y.S., L.X., and X.Z.; investigation, Y.S. and X.Z.; resources, L.X.; writing—original draft preparation, Y.S., L.X., and X.Z.; writing—review and editing, Y.L., F.W., and X.L.; visualization, F.W.; supervision, L.X.; project administration, L.X.; funding acquisition, L.X. All authors have read and agreed to the published version of the manuscript.

Funding: This research was funded by the University of Science and Technology Liaoning College Students' Innovation and Entrepreneurship Training Program Project (X202510146060; 2026).

Institutional Review Board Statement: Not applicable.

Informed Consent Statement: Not applicable.

Data Availability Statement: All relevant data are within the paper.

Acknowledgments: The authors are grateful for the calculation support provided by the Key Laboratory of Molecular Oil Refining of Research Institute of Petroleum Processing in SINOPEC.

Conflicts of Interest: Author Yan Li was employed by the company Delin Land Port Supply Chain Services Co., Ltd. of Ansteel Group Corporation. The remaining authors declare that the research was conducted in the absence of any commercial or financial relationships that could be construed as a potential conflict of interest.

References

1. Sunardi, A.B.T.; Choirunnisa, F.; Dewi, A.S.P.; Widiyandari, H.; Astuti, Y.; Arutanti, O.; Salim, A.A.; Mufti, N. Enriched photocatalytic degradation of methylene orange dye using carbon quantum dots surface-decorated TiO_2 nanocomposites. *Mater. Chem. Phys.* **2025**, *329*, 130049. [CrossRef]
2. Awarasang, S.; Hung, J. Titanium oxide coating on copper surface by electrical discharge coating with hydrogen peroxide-DI water dielectric. *Surf. Coat. Technol.* **2025**, *502*, 131957. [CrossRef]
3. Guo, W.; Chen, W.; Wang, Z.; Mao, Y. Study on Friction Reduction and Photocatalytic Properties of nano-ZnO/TiO_2 Composite Lubricants. *J. Mater. Eng. Perform.* **2024**, *34*, 14822–14831. [CrossRef]
4. Sharma1, B.P.; Sharma, S.S.; Yadav, A.; Khatri, R.; Yadav, S.K. Optimizing the effect of TiO_2 nano powder in water-based paint manufacturing using response surface methodology. *Sci. Rep.* **2025**, *15*, 37072. [CrossRef] [PubMed]
5. Kim, N.; Kim, Y.; Yun, J.; Jeong, S.; Lee, S.; Lee, B.; Shim, J. Surface Coating of Titanium Dioxide Nanoparticles with a Polymerizable Chelating Agent and Its Physicochemical Property. *ACS Omega* **2023**, *8*, 18743–18750. [CrossRef]
6. Mustafa, W.A.A.; Dassenoy, F.; Sarno, M.; Senatore, A. A review on potentials and challenges of nanolubricants as promising lubricants for electric vehicles. *Lubr. Sci.* **2022**, *34*, 1–29. [CrossRef]
7. Wu, H.; Zhao, J.; Cheng, X.; Xia, W.; He, A.; Yun, J.; Huang, S.; Wang, L.; Huang, H.; Jiao, S.; et al. Friction and wear characteristics of TiO_2 nano-additive water-based lubricant on ferritic stainless steel. *Tribol. Int.* **2018**, *117*, 24–38. [CrossRef]
8. Ma, L.; Ma, L.; Lian, J.; Wang, C.; Ma, X.; Zhao, J. Tribological Behavior and Cold-Rolling Lubrication Performance of Water-Based Nanolubricants with Varying Concentrations of Nano-TiO_2 Additives. *Lubricants* **2024**, *12*, 361. [CrossRef]
9. Ma, L.; Ma, X.; Bai, S.; Zhou, J.; Wang, T.; Zhao, J. Research progress of nanolubrication for rolling process. *Int. J. Adv. Manuf. Technol.* **2023**, *129*, 999–1015. [CrossRef]
10. Du, X.; Wang, X.; You, S.; Wang, Q.; Gong, X. A case study of aggregation behaviors of titanium dioxide nanoparticles in the presence of dodecylbenzene sulfonate in natural water. *J. Environ. Sci.* **2015**, *36*, 84–92. [CrossRef]
11. Guo, L. Study on Dispersion and Surface modification of Nano-Titanium Dioxide. Master's Thesis, Donghua University, Shanghai, China, 2015.
12. Sun, W. Effect of sodium dodecyl benzene sulfonate on migration of nano-TiO_2 in saturated porous media. *J. Chifeng Univ. (Nat. Sci. Ed.)* **2019**, *35*, 10–13.
13. Zhang, Z.; Shen, Z.; Shao, C. Adsorption of Anionic Surfactant SDBS on TiO_2/H_2O and Al-TiO_2/H_2O Interfaces. *J. Chang. Univ. (Nat. Sci. Ed.)* **1996**, *8*, 2–5.
14. Wu, K.; Zhang, Y.; Ge, F.; Huang, X.; Ge, H.; Zhao, Y.; Meng, X.; Dou, B. Corrosion behavior of brass in SCW-SDBS-TiO_2 nanofluid. *J. Alloys Compd.* **2021**, *855*, 157483. [CrossRef]
15. Si, Y.; Liu, H.; Li, N.; Zhong, J.; Li, J.; Ma, D. SDBS-assisted hydrothermal treatment of TiO_2 with improved photocatalytic activity. *Mater. Lett.* **2018**, *212*, 147–150. [CrossRef]
16. Arasu, A.V.; Kumar, D.D.; Khan, I.A. Experimental investigation of thermal conductivity and stability of TiO_2-Ag/water nanocompositefluid with SDBS and SDS surfactants. *Thermochim. Acta* **2019**, *678*, 178308.
17. Zhou, M.; Jia, F.; Yan, J.; Wu, H.; Jiang, Z. Lubrication Performance and Mechanism of Water-Based TiO_2 Nanolubricants in Micro Deep Drawing of Pure Titanium Foils. *Lubricants* **2022**, *10*, 292. [CrossRef]
18. Jin, X.; Ding, X.; Pei, G.; Li, S.; Dong, X.; Yang, X.; Wang, R.; Yu, P.; Lv, X. Exploring the optoelectronic properties of calcium vanadate semiconductors: A combined experimental and DFT study. *Int. J. Miner. Metall. Mater.* **2025**, *32*, 1417. [CrossRef]
19. Ri, S.; Kang, J.; Pak, M.; Ri, M.; Ri, C.; Choe, M.; Ju, K. Theoretical investigation of adsorption characteristics of typical additives for zinc electroplating. *J. Mol. Model.* **2023**, *29*, 296. [CrossRef]
20. Özdemir, E.; Kan, E.; Guo, B.; Pashkovski, E.; Agiral, A.; Yildirim, E. The Role of Polyisobutylene-Bis-Succinimide (PIBSI) Dispersants in Lubricant Oils on the Deposit Control Mechanism. *Polymers* **2025**, *17*, 1041. [CrossRef]
21. Alam, M.A.; Bishwas, R.K.; Mostofa, S.; Jahan, S.A. Impact on preferred orientation and crystal strain behavior of nanocrystal anatase-TiO_2 by X-ray diffraction technique. *S. Afr. J. Chem. Eng.* **2024**, *49*, 348–352. [CrossRef]
22. Islam, M.D.; Aman, S.; Bayzid, T.; Rahaman, M.A.; Podder, U.; Khan, G.M.A.; Alam, M.A. Crystal growth behavior of nanocrystal anatase TiO_2: A Rietveld refinement in WPPF analysis. *Chem. Inorg. Mater.* **2025**, *6*, 100108. [CrossRef]
23. Xia, L.; Long, J.; Zhao, Y.; Wu, Z.; Dai, Z.; Wang, L. Molecular Dynamics Simulation on the Effect of Dispersants on the Aggregation of Lubricant Oxidation Products. *Acta Pet. Sin. (Pet. Process. Sect.)* **2018**, *34*, 658–664.
24. Xia, L.; Long, J.; Zhao, Y.; Wu, Z.; Dai, Z.; Wang, L. Molecular Dynamics Simulation on the Effect of Water and Carboxylic Acid Calcium on the Aggregation of Lubricant Oxidation Products. *Acta Pet. Sin. (Pet. Process. Sect.)* **2019**, *35*, 440–448.
25. Barrera, N.F.; Cabezas-Escares, J.; Muñoz, F.; Muriel, W.A.; Gómez, T.; Calatayud, M.; Cárdenas, C. Fukui Function and Fukui Potential for Solid-State Chemistry: Application to Surface Reactivity. *J. Chem. Theory Comput.* **2025**, *21*, 3187–3203. [CrossRef]
26. Yates, P.P.Z.; Bieger, K. Systematic Approach to Negative Fukui Functions: Its Association with Nitro Groups in Aromatic Systems. *Int. J. Mol. Sci.* **2025**, *26*, 319. [CrossRef]

27. Seminario, J.M.; Concha, M.C.; Politzer, P. Calculation of molecular geometries and energies by a local density functional approach. *Int. J. Quantum Chem.* **1991**, *40*, 249–259. [CrossRef]
28. Yekta, M.; Zanjanchi, M.A.; Roohi, H. Adsorption of HCN, HNC and CH_3CN toxic gases on the M-doped (M = Cr, Fe, Ni and Zn) GaNNS: A DFT-D study. *Colloids Surf. A Physicochem. Eng. Asp.* **2024**, *684*, 133120. [CrossRef]
29. Yogeswari, B.; Deivanayaki, S.; Banu, A.S.; Umadevi, V.; Delcyet, V.R.; Venkatraj, A. Molecular Structural, Spectral and HOMO-LUMO Analysis of Acemetacin in Aqueous Phases: A Density Functional Theory Study. *Asian J. Chem.* **2025**, *37*, 795–803. [CrossRef]
30. Vajiha, B.H.; Arulnangai, R.; Banu, K.G.; Asia, T.H.; Thirugnanasambandham, K.; Ganesamoorthy, R. Synthesis, characterization, DFT, HOMO-LUMO, MEP analysis, and in-silico docking studies of piperidine derivatives. *J. Indian Chem. Soc.* **2025**, *102*, 101679.
31. Sujatha, H.S.; Lavanya, M. An insight to HOMO LUMO aspects in corrosion applications. *Can. Metall. Q.* **2023**, *62*, 761–772.

Disclaimer/Publisher's Note: The statements, opinions and data contained in all publications are solely those of the individual author(s) and contributor(s) and not of MDPI and/or the editor(s). MDPI and/or the editor(s) disclaim responsibility for any injury to people or property resulting from any ideas, methods, instructions or products referred to in the content.